Design of novel microfluidic concentration gradient generators suitable for linear and exponential concentration ranges

Design of novel microfluidic concentration gradient generators suitable for linear and exponential concentration ranges.

Authors and affiliation:

Daniel Friedrich,[a] Colin Please,[b] Tracy Melvin[a*]

[a]Optoelectronics Research Centre, University of Southampton, Highfield, Hampshire. SO17 1BJ, UK.

[b] School of Mathematics, University of Southampton, Highfield, Hampshire. SO17 1BJ, UK.

Tel: +44 23 80596505

Fax: +44 23 80593149

* Correspondence email: tm@orc.soton.ac.uk

Abstract

A novel microfluidic concentration gradient generator is designed where secondary flow, induced via a surface groove, is used to yield a concentration gradient across the output of the microfluidic device. The concentration gradient generator design consists of a single microfluidic channel with two inputs and a single obliquely angled surface groove within the base of the channel to induce the secondary flow and create the concentration gradient. The design allows a concentration gradient to be chosen, either linear or exponential, at the exit of the microfluidic channel with the shape and dimensions of the surface groove within the channel obtained by numerical optimisation. The designed device has a small footprint, suitable for integration within lab-on-a-chip structures for the delivery of a series of an agent to either (i) a single channel and with a concentration gradient or to (ii) a series of reactors with concentrations across a defined range, for bioscience or pharmaceutical screening applications or for chemical reactions.

Keywords

Mixing, microchannel, numerical simulation, concentration gradient, laminar flow

1. Introduction

Microfluidic devices for generating stable concentration gradients are attracting significant interest for bioscience applications. The most well known application of concentration gradient generator devices is for chemotaxis studies (the directed migration of cells along concentration gradients of signalling molecules). Examples include the study of wound healing [1, 2] and the study of the immune response following inflammatory infection [3]. Some of the early studies in these areas were done using macro-scale system, i.e. the Boyden and Zigmund chambers [4, 5]. Concentration gradient generators, on the micron scale have improved spatial and temporal control of the soluble microenvironment along with the potential for automation and integration. This has meant that studies, such as tissue patterning for stem cell research [6], have become possible. A major drawback of all microfluidic concentration gradient generator systems, reported so far, is that the concentration gradients produced are limited in range and/or size and thus not suitable for all applications. Stable concentration gradients in chambers of tens to thousands of micrometres in size, with concentration gradients over several orders of magnitude and which are stable for days are required for bioscience applications [7, 8]. A further drawback is the relative complexity of the structures created so far, meaning that a large device footprint is required for relatively small gradient concentration chambers.

The most promising microfluidic concentration gradient generators for bioscience applications, notably using cellular systems, are those that employ flowing solutions. The reason for this is that agents within the concentration gradient can be absorbed and other agents excreted by the living system, resulting is local depletion of agents and the release of excreted products that could have an impact on the living systems. The most well known of the microfluidic concentration gradient generator devices consists of a symmetric microchannel network modified in terms of the connection to the inlet source to produce outlet concentrations that follow a geometric progression and hence deliver a gradient concentration of agents which flow through a final series of output channels, termed here as the ‘split and recombine’ device [9]. These types of devices have been exploited and refined by input of the channels into a single channel of up to a few millimetres wide to provide various concentration gradients (linear, exponential, parabolic, periodic) [10-12]. Although other microfluidic concentration gradient generators have been reported, these devices also have relatively large fabrication footprints and yield 'static' concentration gradients in a channel between two reservoirs [7, 13, 14].

Although the generation of devices for mixing and generation of concentration gradients for chemical applications is limited (as compared to bioscience applications) such structures are begining to find application for combinatorial chemistry studies [15]. The controlled delivery of fluids within microfluidic channels is an emerging area of interest for both the biology and chemical sciences; the mixing of two or more fluids and transport along channels is evaluated [16-19]. Such systems are finding application for the efficient delivery and mixing of reagents for chemical reactions at the microlitre scale [19]. Here we report a novel approach to design a rather simple microfluidic device

suitable for the generation of linear as well as exponential concentration gradients of 2-4 orders of magnitude with a small fabrication footprint; the application of shaped channels for the 'controlled' transport of agents within microfluidic devices is applied [20]. It is envisaged that these devices will find broad application for microscale applications in chemistry and biology.

The microfluidic concentration gradient generator described in this paper, includes a surface groove for induced secondary (or transverse) flow [21] to transport agent from the source stream to the sink stream in a controlled manner (Figure 1). Like previous microfluidic concentration gradient generators, i.e. the 'split and recombine' device [9], the device is designed to have a series of output channels where agents are mixed (i.e. via transverse molecular diffusion) before introduction into a concentration gradient chamber. Although surface groove induced secondary flow has not previously been exploited to yield a concentration gradient generator, such structures have found application for microfluidic mixing [21, 22], hydrodynamic focusing [23] and for improving the efficiency of the delivery of analytes to sensors within integrated microfluidic devices [24]. Surface grooves are useful for the induction of secondary flow because the flow resistance is inversely proportional to the cube of the channel height. If the surface grooves are obliquely angled into the channel, then the main axial flow and the transverse secondary flow together yield a helical flow profile along the channel. Such devices perform effectively where the Reynolds number $Re < 100$. A number of previous theoretical studies have shown that parameters such as the groove angle, length and depth have an effect on the secondary flow profile [25]. The strategy taken here is different, the geometry and dimensions of the surface groove in the channel is designed, in order to define the relative fraction of the agent molecules that is transported from the source stream across the width of the channel and thus provide the required concentration gradient.

2. Modelling and numerical methods

2.1 The concentration gradient generator design

The concentration gradient generator design is shown in figure 1. The groove in the base of the channel is designed to transport the agent from right to left across the microfluidic channel by induced secondary flow, and is thus angled also from the right side of the channel. The output is the mean concentration within each of the outlet channels creating a concentration gradient, as shown in figure 1a. These solutions, after mixing, could be fed into a continuous microfluidic chamber providing a concentration gradient, but this is not considered here. The strategy taken is to define a concentration gradient ((i) linear or (ii) exponential) across the outlet channels and achieve this by manipulating the size and shape of the surface groove with the aim of matching the output concentration profile of the output channels with the desired concentration profile using numerical optimisation. Figure 1b is a schematic representation of the flow profile in the groove gradient generator, the parabolic flow profile in the straight parts of the channel is seen. The groove, where the agent is transported by induced secondary flow, results in a distortion of the parabolic flow profile.

Two designs of concentration gradient generators are shown in figure 2, the first with the simple

groove design and the second with the complex groove design. In both cases the microfluidic channel consists of two adjacent inlets, an obliquely angled groove in the bottom of the channel and 10 equally sized outlet channels (labelled 1 to 10 from right to left). The two inlet liquids, the agent solution and buffer, are considered in the model as a concentration profile across the width of the channel: the concentration is 1 for the agent solution at the inlet and 0 for the buffer at the inlet. The agent inlet has a width W_i while the buffer inlet has a width W-W_i. At the interface of the agent and buffer inlet the concentration changes smoothly from 0 to 1 over 4μm through a smooth Heaviside step function. The flow velocity in the channel inlet is assumed to be fully developed, i.e. parabolic flow profile across the width and height of the channel. These concentration and flow conditions at the channel inlet can be achieved by a Y-mixer [26]. Figures S3 and S4 in the supplementary information show such a Y-mixer incorporated with the designed channels and figures S5 and S6 show the resulting concentration gradient. Since there is a limited effect on the concentration gradient, but a significant increase in simulation time, the simplified inlet conditions given above are employed in subsequent simulations. The ratio of the widths of the two inlets is one of the parameters that is variable in the design. The 'surface groove induced' secondary flow is used to transport the agent across the width of the channel. In the first instance the simple groove design (Figure 2a) is evaluated: the surface groove in the base of the channel is defined by four parameters: groove depth H_g, groove length near side L_n, groove length far side L_f and groove offset L_a, which is the parameter that defines the angle of the groove within the microfluidic channel.

The second device shown in Figure 2b, is a refinement of the device shown in figure 2a, the simple groove design, where the groove in the base of the channel is an irregular pentagonal shape with two parallel sides at the channel side walls; the geometry is defined by two further parameters, L_m and W_m; these are illustrated schematically in Figure 2b and the groove is termed the complex groove design.

2.2 Governing equations

The behaviour of the fluid and agents within the microfluidic grooved gradient generator can be described by two partial differential equations: (i) the Navier-Stokes equations and the (ii) convection-diffusion equation.

(i) The Navier-Stokes equations describe the fluid velocity in microfluidic channels [27]. These equations can be derived from the principles of conservation of mass and momentum. For an incompressible Newtonian liquid with constant density ρ and constant kinematic viscosity ν the Navier-Stokes equations are given by

$$\frac{\partial u}{\partial t} + (\boldsymbol{u}\cdot\nabla)\boldsymbol{u} = -\frac{1}{\rho}\nabla p + \nu\nabla^2\boldsymbol{u} \qquad \text{(i)}$$

$$\nabla\cdot\boldsymbol{u} = 0 \qquad \text{(ii)}$$

Where $\boldsymbol{u} = (u, v, w)$ is the fluid flow velocity in the x, y and z direction and p is the pressure. These equations are used to describe the flow behaviour in the concentration gradient generator devices shown in figure 2. At the channel entrance and exit the pressure is set to a constant value, i.e. p_1 and p_2,

respectively, and the viscous stress is zero; this leads to pressure driven flow. At the channel walls the no-slip condition is applied.

For the cases considered here, aqueous solutions of relatively low concentration of the agents are used, the Navier-Stokes equations are independent of the agent concentration, i.e. the fluid flow velocity is independent of the local agent concentration in the grooved gradient generator.

The flow regime of the microfluidic channel is characterised by the Reynolds number

$$Re = \frac{UH}{\nu} \qquad \text{(iii)}$$

where U is the average flow velocity and H the channel height. In the cases considered here the Reynolds number is below 1 and thus the grooved gradient generator is operated in the laminar flow regime: the flow is turbulence free.

(ii) The convective and diffusive transport of the agent molecules in the microfluidic channel can be described by the convection-diffusion equation

$$\frac{\partial C}{\partial t} + (\boldsymbol{u}\cdot\nabla)C = D\nabla^2 C \qquad \text{(iv)}$$

where C is the agent concentration, $\boldsymbol{u}$ is the flow velocity calculated by the Navier-Stokes equations (i) and (ii) and D is the diffusion coefficient.

To gain insight into the relelative magnitude of convection and diffusion the convection-diffusion equation (iv) is nondimensionalised with the following variables:

$$x = H\bar{x},\ \ y = H\bar{y},\ z = H\bar{z},\ C = C_0\bar{C},\ \boldsymbol{u} = \frac{UH}{L}\bar{\boldsymbol{u}}, t = \frac{L}{U}\bar{t} \qquad \text{(v)}$$

Where C_0 is the initial agent concentration and L the channel length. Here the bar indicates the dimensionless variables. With this nondimensionalisation the convection-diffusion equation (iv) is given by

$$\frac{\partial \bar{C}}{\partial \bar{t}} + (\bar{\boldsymbol{u}}\cdot\nabla)\bar{C} = \frac{LD}{H^2U}\nabla^2\bar{C} \qquad \text{(vi)}$$

Where the convective part and the diffusive part are linked by the nondimensional Graetz number given by

$$Gz = \frac{H^2U}{LD} \qquad \text{(vii)}$$

The Graetz number is the ratio between the diffusion time and the convection time. (The Graetz number is related to the Peclet number $Pe=Gz\left(\frac{H}{L}\right)$, which is the ratio between the convection distance and diffusion distance.) The generated concentration profile at the channel outlet depends on the relative magnitude of the convective and diffusive terms which is indicated by the Graetz number [20]. Ideally the Graetz number is kept large so that diffusion plays only a small role compared to convection.

The boundary conditions for the convection-diffusion equation (vi) are given by no flux across channel walls, no diffusive flux across the channel exit and a concentration profile at the channel entrance. This concentration profile is given by

$$\bar{C} = \hat{H}(W_i - \bar{z}) \qquad \text{(viii)}$$

where $\widehat{H}$ is the Heaviside step function and W_i is the agent inlet stream width.

2.3 Tools and Optimisation Methods

The numerical simulations are performed in two steps: (i) the velocity profile of the fluid as it flows through the device is simulated first (see figure 1b and supplementary information, figure S7), and then (ii) the convection and diffusion of analyte molecules between the two inlet streams is considered; this builds upon the data established from step (i). These simulations are performed with the commercial finite element method package COMSOL Multiphysics 3.4 (COMSOL AB, Stockholm, Sweden). The Reynolds number is well below 1 meaning that the devices operate in a stable, laminar flow regime. For the simulations here, the Graetz number is fixed at $Gz = 50$ which corresponds to a flow velocity of about $3 * 10^{-4} ms^{-1}$ for agents with a diffusion coefficient of $D = 5 * 10^{-11} m^2 s^{-1}$, typical for small to medium sized proteins in aqueous solutions.[28]

A mesh convergence study was performed to establish the optimal mesh size to provide solutions with good accuracy. A detailed description of this study is contained in the 'Meshing and model validation' section of the supplementary information. Shown in figure 3 is a plot of the mesh size plotted against the mean error, maximum error and standard deviation for the values obtained versus those for the finest mesh ($2.5*10^5$ elements); this data was obtained for the linear concentration gradient with the complex groove design. From this data, a mesh with $4*10^4$ elements was found to be appropriate for simulation of the channels suitable for both the linear and exponential concentration gradient generation. To further validate the theoretical approach used, a previously reported microfluidic device which had been evaluated both experimentally and theoretically [29] (with a related geometry to those designed here) was assessed using our simulation approach; the results obtained showed very good agreement with the data reported [29] (see supplementary information).

The numerical optimisations over the parameters defining the groove are performed separately for two target concentration gradients: (i) a linear concentration gradient from the input concentration to zero and (ii) an exponential concentration gradient, i.e. the concentration decreases exponentially across the width of the microfluidic channel with a range of three orders of magnitude. The numerical optimisations are performed with the aim of fitting the concentration profile at the channel exit with one of the two target concentration profiles, i.e. linear or exponential. The quality of the fit for the linear concentration profile, is defined as the square error between the target concentration profile and the simulated concentration profile,

$$E_l = \sum_{i=1}^{n} \left(\frac{n-i}{n-1} - c_i \right)^2 \qquad \text{(ix)}$$

where , $E_{l,}$ is the square error of the linear concentration profile, n is the number of outlet channels and c_i is the average simulated outlet concentration in outlet i. c_i is calculated by the velocity-weighted area integral of the agent concentration at the exit of the outlet and normalised with the area integral of the velocity over the exit of the outlet channel.

The square error for the exponential concentration gradient E_e is given by the relative error, where the

error is scaled with the target concentration profile:

$$E_e = \sum_{i=1}^{n} \left(1 - \frac{c_i}{\omega^{1-i}}\right)^2 \qquad \text{(x)}$$

where, ω is the coefficient for the exponential decay. This scaling of the square error for the exponential concentration gradient results in every outlet channel having the same weight for the error function regardless of the magnitude of the target concentration. This is important for the exponential concentration gradient where the concentration in the outlet channels varies by 3 orders of magnitude.

The numerical optimisation over the parameters defining the groove shape is performed by a two stage process. In the first stage, a random search over the complete parameter range is used to identify the most promising parameter sets, *i.e.* parameter sets where the error given by equation (ix) for the linear concentration gradient or by equation (x) for the exponential concentration gradient is below a certain threshold [30]. The random search compared favorably against the more sophisticated simulated annealing routine [31] inbuilt in Matlab. In the second stage the Nelder-Mead algorithm [32] is used to find the local optimum starting from the three most promising parameter sets identified by the random search. The Nelder-Mead algorithm is a direct, local optimisation routine which is very robust and effective. The combination of the global random search with the local Nelder-Mead algorithm results in a robust optimisation routine.

3. Results

3.1 Concentration gradient generator with a simple groove design

Although it has been demonstrated that a single groove in the base of the channel is sufficient to transport agents from one side of the channel to the other [25], the optimal geometry of the device to achieve a defined concentration gradient at a series of outputs (as shown schematically in figure 1a) had not been established. To illustrate our approach, simulations are performed on a model device where the microfluidic channel has a channel height of H=75µm, a channel width of W=300µm and a channel length of L=700µm. The height chosen is typical for microfluidic gradient generators [9] and the width is chosen to achieve a sufficiently strong transverse flow [33]. The initial groove geometry parameters are chosen so that the transverse flow is maximal for this channel height and width. The strongest transverse flow, according to the work of Lynn and Dandy [33], is given for a groove length of L_n=L_f=150µm and a groove depth of H_g=90µm. The initial groove offset is chosen to be L_a=300µm, which is equivalent to an angle of 45° between the upstream groove edge and the channel side wall, and the groove position is 100µm from the inlet. This ensures that the parabolic flow profile is fully developed before it reaches the groove (see figure 1b). This choice of groove requires a channel length of at least 550µm. Thus the chosen channel length of L=700µm allows for an increase in the groove angle and groove length. The length of the outlet channels is L_o=100µm and the exit width is 26µm. The behaviour of the fluid and agents within the microfluidic grooved gradient generator are established by numerical simulation, based upon two partial differential equations: (i) the Navier-Stokes equations and the (ii) convection-diffusion equation, as described in Section 2.2, within the COMSOL

environment described in Section 2.3. The mean concentration of agent from each of the 10 outlet channels is established.

From this starting point, an optimisation routine is followed to provide a linear concentration gradient from the outlet channels. Table 1 shows the upper and lower limits for the variable parameters used in the random search, notably the groove parameters (H_g, L_f, L_a and L_n) and the agent inlet width (W_i) (see figure 2a). First, optimisation using the random search method was performed over 1000 iterations. This corresponds to 200 iterations for each of the five parameters (H_g, L_f, L_a, L_n and W_i) for the simple groove design. In each of the 1000 iterations the five parameters are generated by a random number generator. The random numbers are uniformly distributed in the range given in table 1. This range of parameters (table 1) encompasses the groove with the maximal transverse flow and provides room for variation from this case. Three of the parameter sets, with the lowest error, obtained from the random search were used as the starting points for a Nelder-Mead optimisation with 400 iterations. Following this, the three resulting parameter sets of the Nelder-Mead optimisation are compared and the parameter set with the lowest error is used as a starting parameter set for further optimisation with 500 iterations using the Nelder-Mead optimisation approach. The parameters providing the best linear concentration gradient from the device with a simple groove design are shown in table 2. Figure 4a provides the mean concentration at each output channel and figure 5b shows the agent concentration profile in the y-z plane inside the 10 outlet channels for the linear concentration generator with the groove parameters given in table 2. The simulated concentration gradient is defined by the velocity-averaged outlet concentrations c_i. A similar optimisation method as described above to create a linear concentration gradient was applied for the exponential concentration gradient. The optimisation results using a coarse mesh ($2.5 * 10^4$ mesh elements) provide very good initial values so that an additional Nelder-Mead optimisation with a fine mesh $4* 10^4$ mesh elements) converges in less than 150 iterations. The additional Nelder-Mead optimisation was performed with a finer mesh because the accuracy of the simulations with the coarse mesh ($2.5 * 10^4$ mesh elements) (see Meshing and Model validation section in the supplementary information) is not sufficient to resolve the small concentrations at the perifery of the gradient, i.e. the low concentrations in the outlets 9 and 10. Figure 4b provides the mean concentration at each output channel and figure 5d shows the agent concentration profile in the y-z plane inside the 10 outlet channels for the exponential concentration generator with the simple groove parameters given in table 2. Acceptable design parameters could not be found to achieve either a linear concentration gradient or an exponential concentration gradient (table 2) using the simple groove design (figure 2a, so for this reason, refinement of the device design was crucial; this is described in section 3.2 below.

In order to assess the impact of the simple groove geometry, a simple groove with the dimensions as previously reported by Lynn and Dandy [33] (for mixing) were incorporated into the channel and were iteratively changed, one by one, by substitution with values of those established for the best optimised linear concentration gradient. (see supplementary information 'Influence of groove geometry on the

concentration gradient'). This study revealed that large changes in the dimension of the simple groove have a limited effect on the concentration gradient at the output channels.

3.2 *Microfluidic concentration generator with a complex groove design*

A more complex groove in the base of the microfluidic channel is now considered (Figure 2b). The groove is pentagonal in shape, whereby the groove edge, first encountered by the solution front, disects straight across the channel base. This non-equilateral pentagon is illustrated in Figure 2b, where the two new parameters, L_m and the width of the intersection W_m, are variable and evaluated by optimisation.

The numerical optimisations are performed in a similar manner as for the simple groove shape (see section 3.1). In the random search optimisation routine the 7 parameters (W_i, H_g, L_f, L_n, L_a,W_m and L_m) are generated by a random number generator. These parameters and the resulting error between the target concentration profile and the simulated concentration profile are saved in a data file. The random search routine is performed for 200 iterations for each parameter, e.g. for the complex groove with 7 parameters 1400 random parameter configurations are generated. This large number of iterations is necessary to identify promising parameter sets for the subsequent local optimisation routine. After the random search the three groove parameter sets with the lowest error are used as starting points for the local Nelder-Mead optimisation. The number of iterations of the Nelder-Mead optimisation was fixed to 400 for the first local optimisation and to 500 for the second local optimisation. For these values, which were choosen after preliminary optimisations, the Nelder-Mead optimisation routine has reached a local minimum, i.e. the value of the square error has reached a local minimum. The resulting groove geometries were used in a simulation with a much finer mesh, i.e. $1.5*10^5$ elements, and both the mean error and the standard deviation of the outlet concentrations between the finer mesh and the mesh used in the optimisation are on the order of $4*10^{-4}$.

The results for the linear and exponential cases are shown in figure 4a and b respectively. The simulated concentration gradients agree well in both cases (for the microfluidic channel type shown in figure 2b) with the target concentration gradient, as shown by the low error values in Table 2. The parameters for the optimised device for the complex groove design are also given in table 2 and shown to scale in figure 5e and 5g.

Figure 5f and 5h also shows the agent concentration profile in the y-z plane inside the 10 outlet channels for the linear and exponential concentration generator with the complex groove parameters given in table 2. The height of the interface between the agent and the buffer, where the agent concentration is 0.5, provides a 'ball park' approximation of the concentration of the agent in each outlet channel and an idea of the concentration gradient across the width of the microfluidic channel. It can be seen that the interface between the agent and buffer decreases across the width of the microfluidic channel. However, this decrease is not linear across the width of the microfluidic channel, which shows that the number and size of the outlet channels are crucial for the generation of the

concentration gradient, i.e. the outlet channels collect a certain part of the concentration profile and homogenise it over the height and width of the outlet channel. The data shown in figure 4 is the mean concentration in each outlet. Thus it should be considered that the outlet channel contents are mixed (in the horizontal direction) and the resulting concentrations are those plotted in figure 4a and b.

The impact of the complex groove dimensions were assessed to establish the effect of the pentagonal groove dimensions on the linear concentration gradient eluting from the 10 outlet channels. Starting from a simple groove with the dimensions as previously reported by Lynn and Dandy [33] (for mixing) the dimensions were adjusted to gradually reach those for the optimised values for the complex groove design. (see supplementary information). The last parameter to be adjusted was that for L_m (see figure 2). The scale of the apex of the pentagonal shape in the base of the channel has the most significant effect on the concentration gradient (See figure S12, Supplementary information, Influence of groove geometry on the concentration gradient). Given these findings the effect of the dimensions of W_m and L_m were considered further for both the linear and exponential concentration gradient generation. These two parameters were adjusted by +/- 50μm for W_m and then L_m and the results revealed modest deviations from the target concentration gradient for the linear concentration and the exponential concentration gradient (see supplementary information, figures S14 and S15).

3.3 *Sensitivity analysis of the microfluidic concentration gradient generator for the exponential concentration gradient.*

A simple sensitivity analysis for application of the complex groove to generate the exponential concentration gradient was performed; every groove parameter is either rounded up or down to the nearest micrometre. All combinations where the 7 groove parameters given in table 2 are either rounded up or down result in $2^7 = 1282$ combinations. For each of these 128 parameter sets the concentration profile is calculated and compared with the concentration profile of the exact optimisation results. The resulting error for the exponential concentration gradient for all 128 parameter sets is between 0.304 and 0.362 and thus close to the optimum value of 0.296 (See supplementary information, figure S8). This suggests that the gradient generator design is robust enough to provide a well-defined exponential concentration gradient from a microfluidic channel with the complex groove in the base, fabricated using current microfabrication methods.

The simulation was also performed with a range of Graetz (Gz) numbers between 0.5 and 200 for the complex groove device (shown in figure 2b) having the same parameters as outlined in Section 2.2 (data for Graetz numbers between 5 and 150 is shown in the supplementary information, figure S9). The results obtained hardly changed for Graetz numbers between 25 and 100 as compared to the results shown in figure 4. However, for Graetz numbers of $Gz < 1$, the effect of diffusion begins to become much more important, and the generated concentration profile becomes more uniform across the width of the channel. For Graetz numbers $Gz > 100$ the concentration at the far side of the channel, i.e. at the outlets 8, 9 and 10, decreases due to negligible diffusive transport. The results obtained demonstrate that

the concentration gradient generator with the complex groove shape is insensitive towards slight variations in the flow and diffusion parameters.

4 Discussion

The strategy developed here is to design a microfluidic channel and single surface groove to yield mean concentration outputs from ten channels that are either linear or exponential in concentration range. The approach applied is to first define the required mean concentration at each of the exits of the ten output channels according to the desired concentration gradient and then use numerical simulations to establish the optimal groove shape in the base of the channel to achieve this. A microfluidic channel with two inputs and an obliquely angled, irregular pentagonal groove in the base of the channel can be used to provide output solutions which, after mixing, have a gradient of concentration, as shown in figure 4. The geometry of the optimised irregular pentagonal groove shapes are shown to scale in figure 5. Controlled transfer of agents by secondary induced flow via the lower pentagonal groove is achieved; figure S7 in the supplementary information further illustrates the transfer via the lower pentagonal groove. There is sufficient flexibility with respect to the parameters used to define the irregular pentagonal groove in the base of the channel, that a groove of uniform depth can be applied. As can be seen from figure 5 and the parameters in table 2, it is a combination of the shape of the groove and the agent inlet width that define how much of the agent is delivered to each of the channels. Other complex groove designs for other concentration gradients are theoretically possible, where the same numerical and optimisation approach can be applied.

The fabrication of the concentration gradient generators of the dimensions described here from planar substrates using planar lithography and deep reactive ion-etching techniques, although challenging, is achievable. Furthermore, because the transverse flow in the microfluidic channel depends only on the ratios of the channel and groove geometries, the results are applicable to scaled devices (provided the aspect ratios of the channel and the groove remain unchanged), with the proviso that the flow is stable laminar flow. Thus larger devices could be fabricated using polymer microfabrication methods, and indeed for related devices effective performance where the Reynolds number $Re < 100$ has been reported. [21] Our theoretical investigations do suggest that for Graetz values Gz, of between 25 to 100 (see supplementary information, Figure S9) similar results are obtained and thus the device is relatively insensitive to flow and diffusion parameters. A simple sensitivity analysis, of the complex groove applied for generating an exponential concentration gradient, suggested that the design is insensitive against slight variations resulting from precision of the device fabrication as well as the device operation parameters such as flow rate and diffusion coefficient of the agents.

5. Conclusions

A new philosophy for the design of concentration gradient generators is presented; these structures

consist of simple channels with a groove of relatively complex geometry in the base. The numerical optimisation results demonstrate linear or exponential concentration gradients can be created using pentagonal groove shapes, which are used to induce specified secondary flow transversely to the bulk flow direction. Whilst it is well known that the secondary flow profile is dependent on the size of the surface groove, here, for the first time, the size and shape of the surface groove is considered with a view to achieve the controlled transport of agent molecules across the width of the microfluidic channel.

The key advantage of the concentration gradient generator is the requirement for only one mixing stage, and as a consequence the device is relatively small. If compared to the 'split and recombine' gradient generator, which requires at least $\log_2(n-1)$ mixing stages to create n different outlet channels, the device is much shorter and narrower and consequently requires less chip real-estate. The other advantage is the facility to produce both linear and exponential concentration gradients. A further advantage is the scalability of the device, provided that the Reynolds number is ≤ 100. Such structures are likely to be of significant application for bioscience applications, but it is also envisaged that such structures will be suitable for integration within lab-on-a-chip structures where combinatorial chemistry, pharmaceutical or biochemistry assays are performed.

Nomenclature

C	agent concentration (M)
D	diffusion coefficient (m^2s^{-1})
Gz	Graetz number ($Gz = \frac{H^2U}{LD}$)
H	channel height (m)
$\hat{H}$	Heaviside step function
L	channel length (m)
p	pressure (Nm^{-2})
Pe	Peclet number ($Pe=Gz\left(\frac{H}{L}\right)$)
U	average flow velocity (ms^{-1})
Re	Reynolds number ($=UH/\nu$)
t	time (s)
$\boldsymbol{u} = (u, v, w)$	fluid flow velocity in the x, y and z direction
W	main channel width (m)
W_i	agent inlet width (m)
x,y,z	coordinates

Greek letters

ρ	density (kgm^{-3})
ν	kinematic viscosity (Nsm^{-2})

Figure Legends

Figure 1. Schematic representation of the grooved concentration gradient generator.

(a) Transport of the solubilised agent (red) and the buffer (blue) by secondary flow along the groove across the width of the channel. The solubilised agent and the buffer are introduced as separate streams by pressure-driven flow into the grooved concentration gradient generator channel. Ten equal-width outlet channels are at the exit of the grooved concentration gradient generator. The method allows for the design of the generator where the mean agent concentration at each outlet is considered, even if at each outlet channel the agent is not uniformly distributed across the height and width of each outlet channels.

(b) Flow profile in the grooved gradient generator: shown is the velocity field which is a combination of the flow velocities in the x, y and z direction. The velocity increases from blue to red.

Figure 2**.** The design of the grooved gradient generator: 3D schematic of (a) the simple groove design, (b) the complex groove design.

Figure 3. Plot of mesh size versus the mean error, maximum error and standard deviation for the simulation results obtained versus those obtained with the finest grid (2.5×10^5) for the linear concentration gradient with the complex groove design.

Figure 4. (a) Plot of the target and the simulated (and optimised) mean concentration at each output channel; appropriate for an output with a linear concentration gradient from (i) the microfluidic channel with the simple groove design, (ii) the microfluidic channel with the complex groove design. (b) Semi-log plot of the target and the simulated and optimised mean concentration at each output channel; appropriate for an exponential concentration gradient from (i) the microfluidic channel with the simple groove design, (ii) the microfluidic channel with the complex groove design. Parameters: $Gz = 50, \omega = 2$.

Figure 5. (a) Optimal design (to scale) of the simple groove shape within the channel required to achieve a linear concentration gradient. (b) Plot of the agent concentration in the outlet channels of a gradient generator for a linear concentration gradient. The mean agent concentration decreases from outlet channel 1 to 10. Parameters: $Gz = 50$ (c) Optimal designs (to scale) of the simple groove shape within the channel required to achieve an exponential concentration gradient. (d) Plot of the agent concentration in the outlet channels of a gradient generator for an exponential concentration gradient. Parameters: $Gz = 50, \omega = 2$ (e) Optimal design (to scale) of the complex irregular pentagonal groove shapes within the channel required to achieve a linear concentration gradient. (f) Plot of the agent concentration in the outlet channels of a gradient generator for a linear concentration gradient. The mean agent concentration decreases from outlet channel 1 to 10. Parameters: $Gz = 50$ (g) Optimal designs (to

scale) of the complex irregular pentagonal groove shape within the channel required to achieve an exponential concentration gradient. (h) Plot of the agent concentration in the outlet channels of a gradient generator for an exponential concentration gradient. Parameters: $Gz = 50, \omega = 2$

Table Legends

Table 1. Lower and upper limit of the parameters used for the random search for the simple and complex groove design. (See Figure 2 for reference of parameter notation)

Table 2. Results of the optimisation for the simple and complex groove shape and for the linear and exponential concentration gradient. The error is obtained using equations (ix) and (x), where the parameters $Gz = 50, \omega = 2$.

References

[1] H.L. Ashe, J. Briscoe, The interpretation of morphogen gradients, Development, 133 (2006) 385-394.
[2] R.A. Firtel, C.Y. Chung, The molecular genetics of chemotaxis: sensing and responding to chemoattractant gradients, Bioessays, 22 (2000) 603-615.
[3] X.D. Yang, J.R.F. Corvalan, P. Wang, C.M.N. Roy, C.G. Davis, Fully human anti-interleukin-8 monoclonal antibodies: potential therapeutics for the treatment of inflammatory disease states, Journal of Leukocyte Biology, 66 (1999) 401-410.
[4] S. Boyden, The chemotactic effect of mixtures of antibody and antigen on polymorphonuclear leucocytes., Journal of Experimental Medicine, 115 (1962) 453-466.
[5] S.H. Zigmond, J.G. Hirsch, Leukocyte Locomotion and Chemotaxis - New Methods for Evaluation and Demonstration of a Cell-Derived Chemotactic Factor, Journal of Experimental Medicine, 137 (1973) 387-410.
[6] L. Kim, M.D. Vahey, H.Y. Lee, J. Voldman, Microfluidic arrays for logarithmically perfused embryonic stem cell culture, Lab on a Chip, 6 (2006) 394-406.
[7] W. Saadi, S.W. Rhee, F. Lin, B. Vahidi, B.G. Chung, N.L. Jeon, Generation of stable concentration gradients in 2D and 3D environments using a microfluidic ladder chamber, Biomedical Microdevices, 9 (2007) 627-635.
[8] B.G. Chung, L.A. Flanagan, S.W. Rhee, P.H. Schwartz, A.P. Lee, E.S. Monuki, N.L. Jeon, Human neural stem cell growth and differentiation in a gradient-generating microfluidic device, Lab on a Chip, 5 (2005) 401-406.
[9] N.L. Jeon, S.K.W. Dertinger, D.T. Chiu, I.S. Choi, A.D. Stroock, G.M. Whitesides, Generation of solution and surface gradients using microfluidic systems, Langmuir, 16 (2000) 8311-8316.
[10] S.K.W. Dertinger, D.T. Chiu, N.L. Jeon, G.M. Whitesides, Generation of gradients having complex shapes using microfluidic networks, Analytical Chemistry, 73 (2001) 1240-1246.
[11] F. Lin, W. Saadi, S.W. Rhee, S.J. Wang, S. Mittal, N.L. Jeon, Generation of dynamic temporal and spatial concentration gradients using microfluidic devices, Lab on a Chip, 4 (2004) 164-167.
[12] K. Campbell, A. Groisman, Generation of complex concentration profiles in microchannels in a logarithmically small number of steps, Lab on a Chip, 7 (2007) 264-272.
[13] B. Mosadegh, C. Huang, J.W. Park, H.S. Shin, B.G. Chung, S.K. Hwang, K.H. Lee, H.J. Kim, J. Brody, N.L. Jeon, Generation of stable complex gradients across two-dimensional surfaces and three-dimensional gels, Langmuir, 23 (2007) 10910-10912.
[14] C.W. Li, R.S. Chen, M.S. Yang, Generation of linear and non-linear concentration gradients along microfluidic channel by microtunnel controlled stepwise addition of sample solution, Lab on a Chip, 7 (2007) 1371-1373.
[15] Y.H. Jang, M.J. Hancock, S.B. Kim, S. Selimovic, W.Y. Sim, H. Bae, A. Khademhosseini, An integrated microfluidic device for two-dimensional combinatorial dilution, Lab on a Chip, 11 (2011) 3277-3286.
[16] K.-I. Sotowa, K. Takagi, S. Sugiyama, Fluid flow behavior and the rate of an enzyme reaction in deep microchannel reactor under high-throughput condition, Chemical Engineering Journal, 135 (2008) S30-S36.
[17] A. Cantu-Perez, S. Barrass, A. Gavriilidis, Hydrodynamics and reaction studies in a layered herringbone channel, Chemical Engineering Journal, 167 (2011) 657-665.
[18] K.-I. Sotowa, A. Yamamoto, K. Nakagawa, S. Sugiyama, Indentations and baffles for improving mixing rate in deep microchannel reactors, Chemical Engineering Journal, 167 (2011) 490-495.
[19] M.M.E. Delville, P.J. Nieuwland, P. Janssen, K. Koch, J.C.M. van Hest, F.P.J.T. Rutjes, Continuous flow azide formation: Optimization and scale-up, Chemical Engineering Journal, 167 (2011) 556-559.

[20] D. Friedrich, C. Please, T. Melvin, Optimisation of analyte transport in integrated microfluidic affinity sensors for the quantification of low levels of analyte, Sensors and Actuators B-Chemical, 131 (2008) 323-332.
[21] A.D. Stroock, S.K.W. Dertinger, A. Ajdari, I. Mezic, H.A. Stone, G.M. Whitesides, Chaotic mixer for microchannels, Science, 295 (2002) 647-651.
[22] A.D. Stroock, S.K. Dertinger, G.M. Whitesides, A. Ajdari, Patterning flows using grooved surfaces, Analytical Chemistry, 74 (2002) 5306-5312.
[23] P.B. Howell, J.P. Golden, L.R. Hilliard, J.S. Erickson, D.R. Mott, F.S. Ligler, Two simple and rugged designs for creating microfluidic sheath flow, Lab on a Chip, 8 (2008) 1097-1103.
[24] J.P. Golden, T.M. Floyd-Smith, D.R. Mott, F.S. Ligler, Target delivery in a microfluidic immunosensor, Biosensors & Bioelectronics, 22 (2007) 2763-2767.
[25] D.R. Mott, P.B. Howell, J.P. Golden, C.R. Kaplan, F.S. Ligler, E.S. Oran, Toolbox for the design of optimized microfluidic components, Lab on a Chip, 6 (2006) 540-549.
[26] A.E. Kamholz, P. Yager, Theoretical analysis of molecular diffusion in pressure-driven laminar flow in microfluidic channels, Biophysical Journal, 80 (2001) 155-160.
[27] D.J. Acheson, Elementary Fluid Dynamics, Clarendon Press, Oxford and New York, 1990.
[28] H.A. Sober, CRC Handbook of Biochemistry, in: H.A. Sober (Ed.), CRC Press, Cleveland, Ohio, 1970.
[29] P.B. Howell, Jr., D.R. Mott, F.S. Ligler, J.P. Golden, C.R. Kaplan, E.S. Oran, A combinatorial approach to microfluidic mixing, Journal of Micromechanics and Microengineering, 18 (2008).
[30] M. Aoki, Introduction to Optimization Techniques - Fundamentals and Applications of Nonlinear Programming Macmillan, New York, 1971.
[31] S. Kirkpatrick, C.D. Gelatt, M.P. Vecchi, Optimization by Simulated Annealing, Science, 220 (1983) 671-680.
[32] J.C. Lagarias, J.A. Reeds, M.H. Wright, P.E. Wright, Convergence properties of the Nelder-Mead simplex method in low dimensions, Siam Journal on Optimization, 9 (1998) 112-147.
[33] N.S. Lynn, D.S. Dandy, Geometrical optimization of helical flow in grooved micromixers, Lab on a Chip, 7 (2007) 580-587.

Table 1

Description	Parameter	Lower limit	Upper limit
Agent inlet width	W_i	20µm	200µm
Groove depth	H_g	20µm	100µm
Groove length far side	L_f	10µm	220µm
Groove length near side	L_n	100µm	450µm
Groove offset	L_a	100µm	370µm
Sidewall to apex length.	W_m	50 µm	210µm
Groove length at irregular pentagon apex.	L_m	50µm	360µm

Table 2

	Simple linear	Simple exponential	Complex linear	Complex exponential
W_i	152.9µm	65.6µm	143.9µm	66.9µm
H_g	71.6µm	32.4µm	98.5µm	51.7µm
L_f	217.7µm	168.0µm	195.0µm	38.8µm
L_n	394.5µm	268.0µm	149.5µm	371.2µm
L_a	360.4µm	302.0µm	249.8µm	301.2µm
W_m	n\a	n\a	141.2µm	142.8µm
L_m	n\a	n\a	377.8µm	322.8µm
Error	0.142	1.544	0.014	0.296

Figure 1

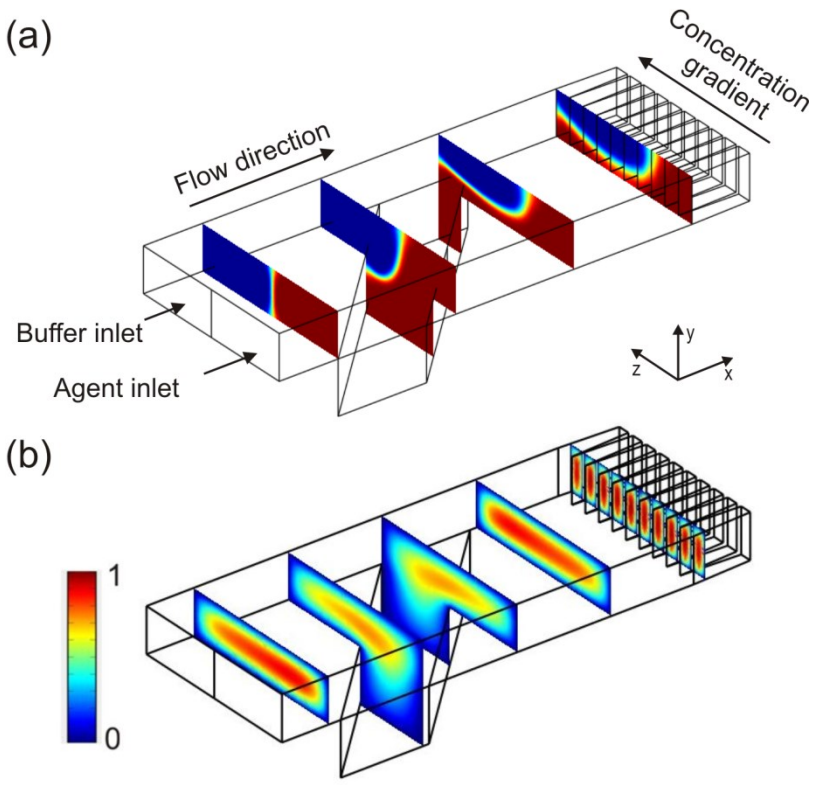
(a)
Concentration gradient
Flow direction
Buffer inlet
Agent inlet
y
z
x
(b)
1
0

Figure 2

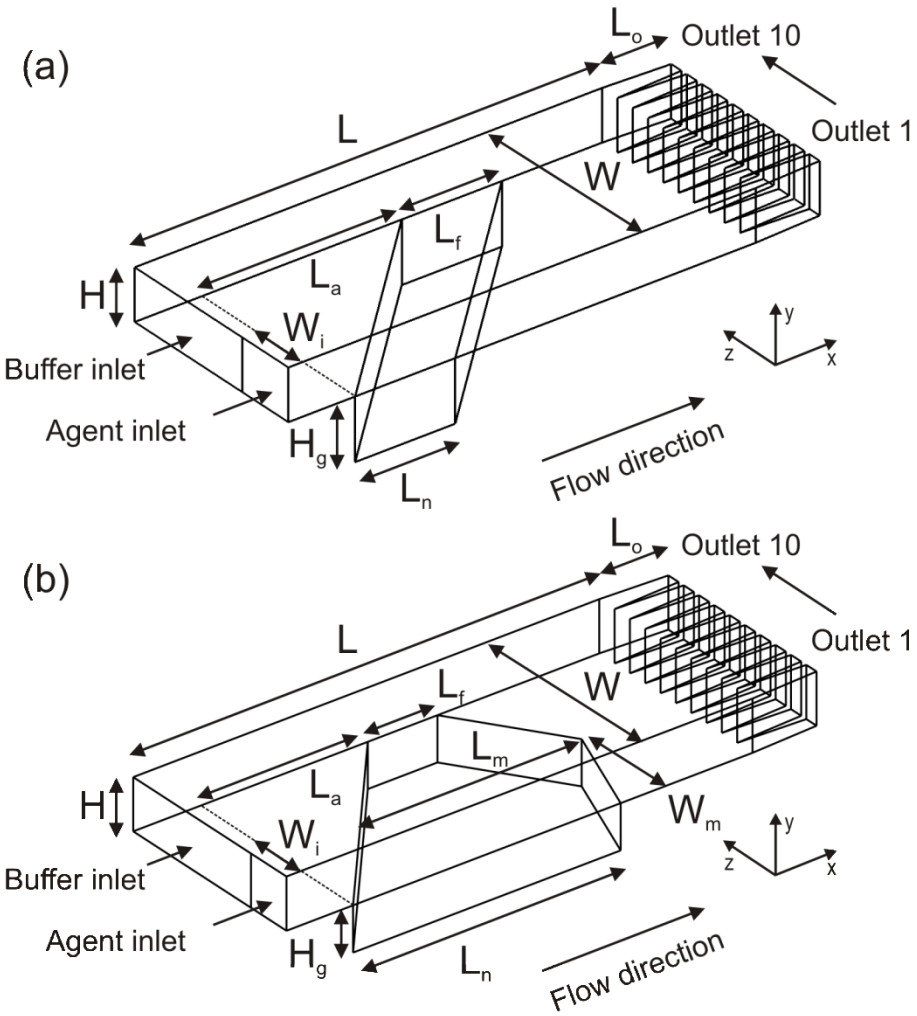
(a)
L_o
Outlet 10
Outlet 1
L
W
L_f
L_a
H
W_i
Buffer inlet
Agent inlet
H_g
L_n
Flow direction
y
z
x
(b)
L_o
Outlet 10
Outlet 1
L
L_f
W
L_m
L_a
H
W_m
W_i
Buffer inlet
Agent inlet
H_g
L_n
Flow direction
y
z
x

Figure 3

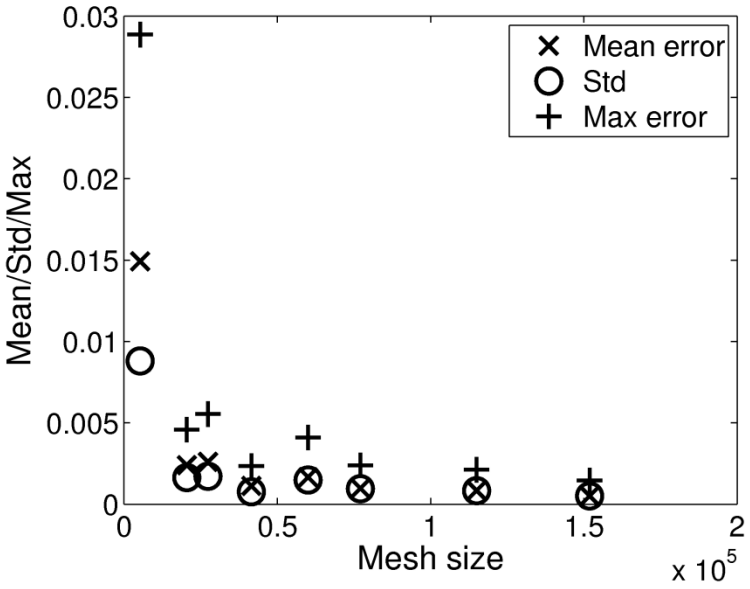
Mean error
Std
Max error
Mean/Std/Max
Mesh size
x 10^5
0.03
0.025
0.02
0.015
0.01
0.005
0
0.5
1
1.5
2

Figure 4

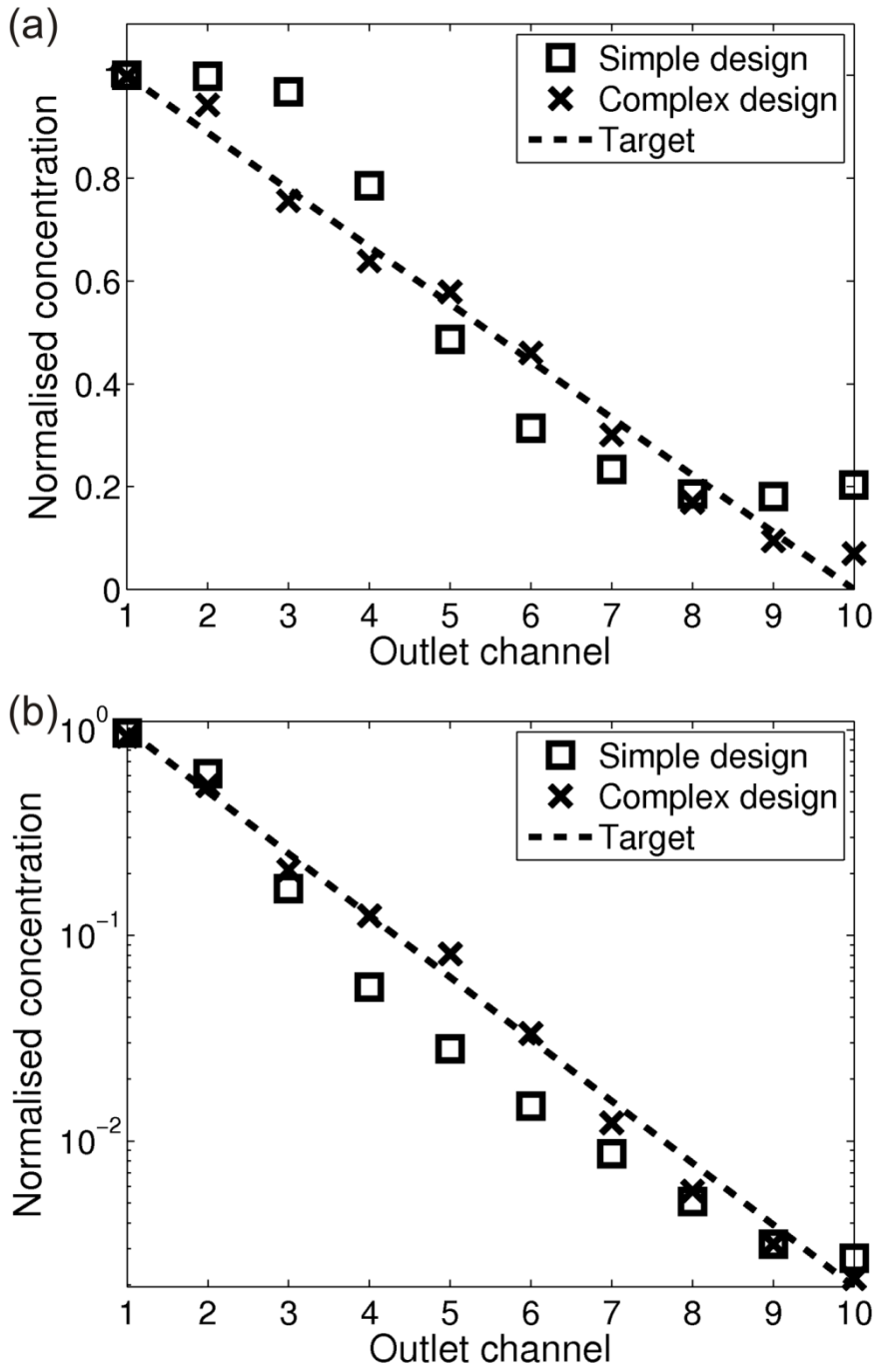
(a)
Simple design
Complex design
Target
Normalised concentration
0
0.2
0.4
0.6
0.8
1
2
3
4
5
6
7
8
9
10
Outlet channel
(b)
Simple design
Complex design
Target
Normalised concentration
10^{0}
10^{-1}
10^{-2}
1
2
3
4
5
6
7
8
9
10
Outlet channel

Figure 5

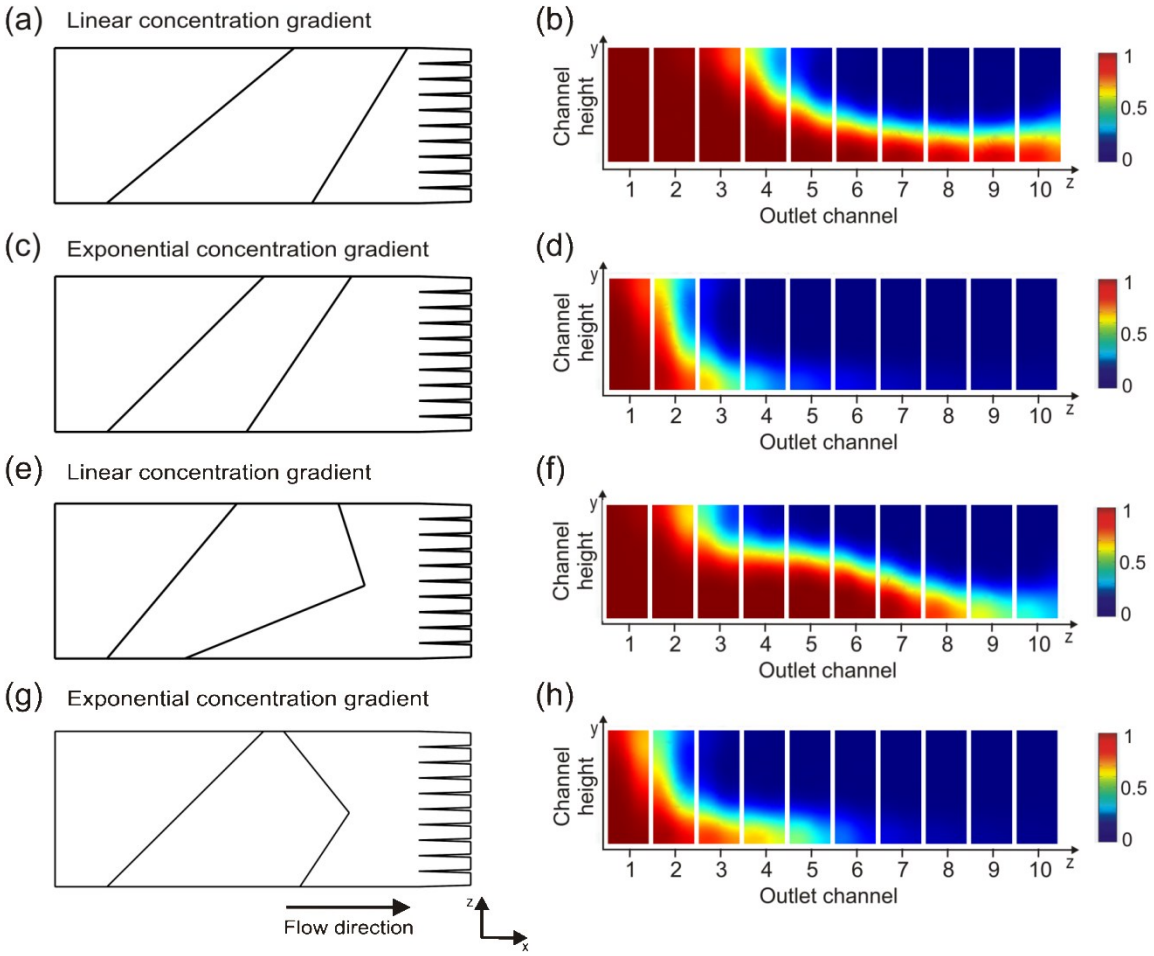
(a) Linear concentration gradient
(b)
(c) Exponential concentration gradient
(d)
(e) Linear concentration gradient
(f)
(g) Exponential concentration gradient
(h)
Channel height
Outlet channel
Flow direction
y
z
x
1
0.5
0
1 2 3 4 5 6 7 8 9 10

Supplementary information: Grooved gradient generator

Daniel Friedrich,[a] Colin Please[b] and Tracy Melvin*[a]

[a] *Optoelectronics Research Centre, University of Southampton, Highfield, Hampshire, SO17 1BJ, UK*
[b] *School of Mathematics, University of Southampton, Highfield, Hampshire, SO17 1BJ, UK*

Implementation details

The numerical simulations of the behaviour of the grooved gradient generator are composed of two steps: (i) first the steady flow profile is simulated and (ii) the convection and diffusion of agent molecules is simulated with the flow profile from step (i). These simulations are performed with the commercial finite element method package COMSOL Multiphysics 3.4 (COMSOL AB, Stockholm, Sweden). The error between the resulting concentration profile and the target concentration profile is calculated with equation (ix) or (x) which are given in the main text. These steps are implemented in a COMSOL script.

The random search and the Nelder-Mead optimisation routines, which call this COMSOL script, are performed in the Matlab environment (The Mathworks, Natick, MA, USA). All simulations are performed on a computer with a Dual Core AMD Opteron Processor 880 2.4 GHz and 8 GB of main memory.

COMSOL script for the simulation of the grooved gradient generator

The COMSOL script used by the optimisation routines is created in a two stage process. In the first stage the graphical user interface (GUI) of COMSOL is used to create the geometry, physics model, mesh and solver setup. This COMSOL model is then exported as a Matlab script which is modified by hand in the second stage. The main steps in this second stage are the insertion of variables defining the device geometry and the calculation of the square error between the target concentration profile and the simulated concentration profile.

GUI model

The COMSOL GUI provides a simple and easy to learn interface for the setup of complex multiphysics problems in a step by step manner. First, the 3D geometry is defined through a simple computer-aided design tool. For the system considered here, see figure 1 in the main text, the geometry is uniform in the y direction. Using this the outline of the device in the x-z plane is drawn (see figure 2 in the main text) and extruded in the y direction.

In the second step, the physics models for the incompressible Navier-Stokes equations (i) and (ii) and the convection-diffusion equation (iv) are defined. Both are available from the 'Model Navigator' in the basic COMSOL module. The simulations are performed for aqueous solutions at room temperature (T=25° C) so the density and dynamic viscosity of water are given by: $\rho=997.13 kgm^{-3}$, $\mu=0.891*10^{-3} kgm^{-1}s^{-1}$. The boundary conditions are set to a constant pressure at the inlet ('Pressure, no viscous stress'), atmospheric pressure at the outlet ('Pressure, no viscous stress') and the no-slip condition at the channel walls. The solution of the Navier-Stokes equations is used as the velocity vector in the convection-diffusion equation.

The boundary conditions for the convection-diffusion equation of the agent molecules are set to 'Insulation/Symmetry' at the channel walls, 'Convective flux' at the outlets and 'Concentration' at the channel inlet. The concentration profile at the channel inlet defines the width of the agent and buffer stream, i.e. the concentration in the agent stream is set to 1 while the concentration in the buffer stream is set to 0. However, this step in the inlet concentration boundary condition poses problems for the numerical solution of the convection-diffusion equation. By replacing the discontinuous step function with a smooth step function the numerical properties of the system are improved. The resulting system is more stable and the convergence properties are enhanced. Furthermore, in the physical system the discontinuous step in the input concentration is smoothed to a continuous step immediately after the two streams merge. Here the inbuilt function 'flc1hs' which is a smoothed Heaviside step function without overshoot is used. The distance over which the smoothing occurs is set to 4µm. This is a reasonable choice because for a diffusion coefficient $D=5*10^{-11} m^2s^{-1}$ the agent molecules diffuse this distance in less than 0.2 seconds.

The meshing of the geometry is performed with the default values provided by COMSOL. Later, this default mesh is analysed and improved to achieve the desired accuracy in the solution. The last step, the solving of the physics model is performed sequentially. This is possible because the flow velocity for aqueous solutions is independent of the agent concentration. First, the Navier-Stokes equations are solved with the default static solver ('gmres'). Second, the convection-diffusion equation is solved for the flow velocity calculated in the first step. The convection-diffusion equation is solved with the static 'spooles' solver. The completed GUI model is then exported as a Matlab script.

Modification of the Matlab script

The Matlab script containing the GUI model is modified by hand. The numerical values defining the channel and groove geometry are replaced by variables for the channel dimensions (height, width, length, groove start, inlet width) and the groove dimensions: groove depth H_g, groove length near side L_n, groove length far side L_f, groove offset L_a groove midpoint W_m and groove length at the midpoint L_m. This simplifies the modification of the channel and groove dimensions and allows the optimisation over the groove parameters. The additional variables 'inlet_mesh',

'wall_mesh_fine' and 'wall_mesh' which define the maximal mesh size at the channel inlet, the channel outlets and the channel wall, respectively, are introduced.

Furthermore, the area integral of the velocity weighted agent concentration at the channel outlets is calculated and normalised with the size of the channel outlets. In the last step, the square error between the target concentration profile and the simulated concentration profile is calculated and returned to the optimisation routine.

Meshing and model validation

Meshing is very important for the accuracy and convergence of FEM simulations. This is especially true for 3D simulations. However, the problem considered here is numerically stable because the dominant concentration gradient is across streamlines rather than along streamlines.

Here two strategies for the mesh generation are used to ensure an accurate solution of the problem. First, the maximal size of the mesh elements at the boundaries of the microfluidic channel, especially at the inlet and the outlet channels, is restricted. This is necessary because the flow velocity changes considerably close to the channel walls and the interface between the agent and buffer is most important at the inlet and outlets. The second strategy uses the adaptive mesh refinement from COMSOL. Using this in the calculation of the convection-diffusion problem refines the mesh at the interface between the two input streams where the largest gradient in the concentration occurs.

A mesh convergence study which compares the simulated concentration gradient for different mesh sizes was performed. A preliminary mesh convergence study was performed with a non-optimised surface groove. This study suggested that $2.5*10^4$ mesh elements which result in about $1.3*10^5$ degrees of freedom, i.e. the size of the system of equations, are sufficient for an accuracy of 10^{-3} in the normalised outlet concentration c_i. The optimisations for the linear and exponential concentration gradients were performed with this mesh. A further mesh convergence study was performed for the optimised surface grooves. Here, the mesh size was increased from about $2.5*10^4$ elements to $2.5*10^5$ elements which increases the simulation time by fifty-fold. The mean error and standard deviation of the solutions of the coarse mesh simulations compared to the fine mesh simulation are shown in table T1. This mesh convergence study shows that for the linear concentration gradient a mesh with $2.5*10^4$ elements produces a result with sufficient accuracy, i.e. the mean error is much lower than the target agent concentrations. However, for the exponential concentration gradient which requires an accuracy to three significant figures a finer mesh is required. The results from table T1 suggest that a mesh with about $4*10^4$ elements is sufficient for the exponential concentration gradient. Thus for the exponential concentration gradient a further Nelder-Mead optimisation with this finer mesh and the results of the first optimisation as initial values is performed. This optimisation converges in less than 150 iterations. The results of this optimisation were compared to the results of a finer mesh with $1.5*10^5$ elements. The mean error over the 10 outlet channels is $4.3*10^{-4}$ with a standard deviation of $4.3*10^{-4}$ so that the mesh with $4*10^4$ elements is sufficient for this exponential concentration gradient.

Table T1 Comparison of the simulation results for the coarse meshes with the fine mesh for the linear concentration gradient. The mean error and standard deviation of the 10 outlet channels compared to the values for the finest grid are shown. While the shown computation time depends on the used computer, it gives an indication of the relative computation time for the different mesh sizes.

Mesh size	System size	Mean error	Standard deviation	Computation time
$2*10^4$	10^5	$2.4*10^{-3}$	$1.6*10^{-3}$	2 min
$2.5*10^4$	$1.3*10^5$	$2.6*10^{-3}$	$1.7*10^{-3}$	3 min
$4*10^4$	$2*10^5$	$1.1*10^{-3}$	$0.8*10^{-3}$	5 min
$6*10^4$	$3*10^5$	$1.7*10^{-3}$	$1.5*10^{-3}$	10 min
$1.5*10^5$	$7*10^5$	$0.5*10^{-3}$	$0.5*10^{-3}$	57 min

To gain further confidence in the simulation results the same model setup and simulation routine was used to simulate a device already reported in the literature (see reference 29). The device is represented in figure S1 and the dimensions used are as published (reference 29). The outlet concentration profile as calculated using our approach is shown in figure S2.

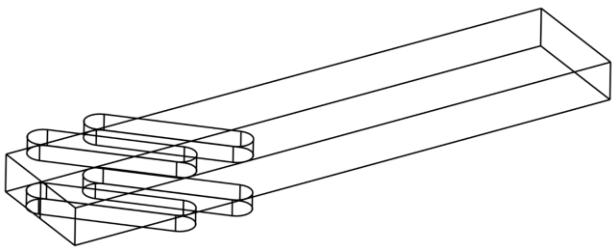

Fig.S1 Schematic of the simulated device from ref. 29 (Parameters used for the simulation: Channel width:3.175mm, channel height:1.016mm, groove depth: 0.432mm, groove length: 0.794mm, Reynolds number<100) (All other aspects are to scale.)

The results shown in figure S2 compare very favourably with the

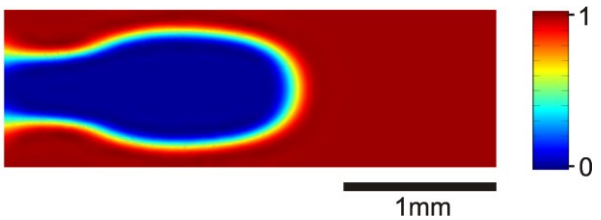

Fig.S2 Concentration outflow profile at the channel outlet as a cross-section. The scale bar is concentration fraction for the right hand inlet solution versus the left hand inlet solution.

experimental data presented by Howell *et al.* in reference 29, (See figure 4 in that article). In addition the data generated by our simulation approach (Fig. S2) is in agreement with data also shown by Howell *et al.* (figure 4 in ref. 29), but simulated by a different method.

Random search and Nelder-Mead optimisation

The optimisation over the size of the groove is performed in the Matlab environment. The two optimisation routines, random search and the Nelder-Mead optimisation, define the groove geometry through the device parameters (see Figure 2) and call the COMSOL script. The COMSOL script calculates the concentration profile for the given groove parameters and returns the square error between the simulated and target concentration profile.

Effects of the channel inlet

The simulations are performed with a fully developed flow profile at the channel inlet and a smooth concentration step at the position given by the inlet width.

This step is given by a smoothed Heaviside step function, i.e. the transition from c=0 to c=1 takes place over 4um. This configuration simplifies the numerical simulations considerably compared to a simulation taking two inlet streams into account. However, to achieve such inlet conditions requires a Y-mixer upstream of the simulated microfluidic channel.

Figures S3 and S4 show the complex design of the gradient generator with a Y-mixer. The width of the agent inlet channel in the Y-mixer is given by the inlet width from the optimisation. The average flow rate in the agent and buffer arm of the Y-mixer are choosen to correspond to the average flow rate of the agent and buffer part of the simplified inlet conditions.

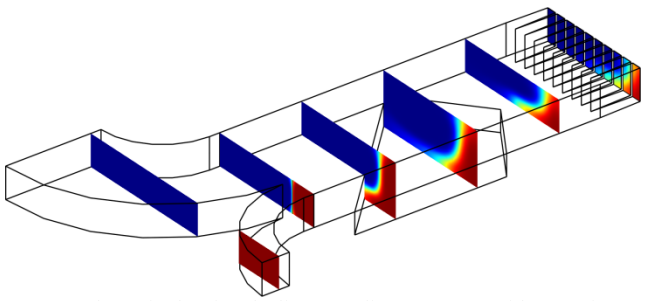

Fig. S3 Schematic showing the linear gradient generator with a Y-mixer and the agent concentration along the channel.

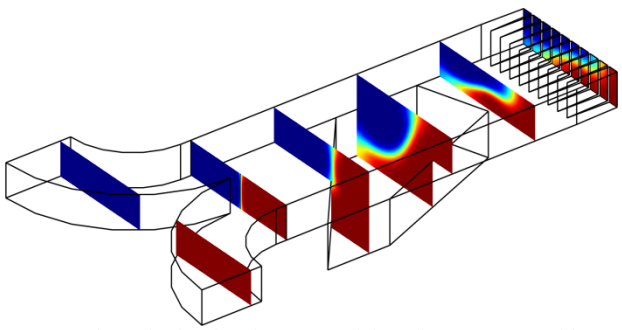

Fig. S4 Schematic showing the exponential gradient generator with a Y-mixer and the agent concentration along the channel.

The resulting concentration gradient is in very good agreement with the simulations performed with the simplified inlet conditions, see figures S5 and S6. The calculated errors are 0.0213 and 0.2151 for the linear and exponential concentration gradient, respectively. These values compare favourably with errors given in table 2 in the main text.

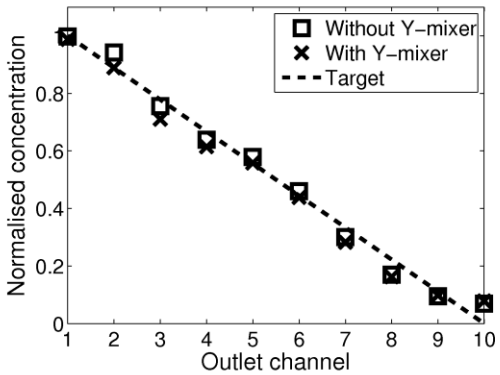

Fig. S5 Simulated linear concentration gradient for the complex groove geometry with and without a Y-mixer.

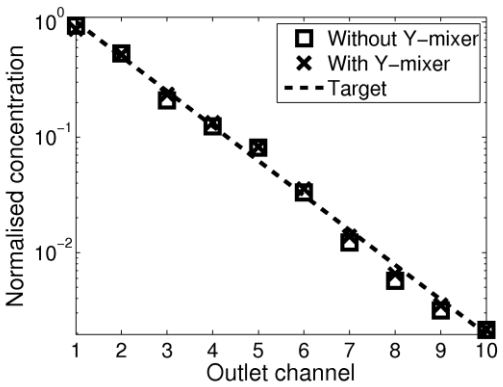

Fig. S6 Simulated exponential concentration gradient for the complex groove geometry with and without a Y-mixer.

Flow profile

The effect of the surface groove on the streamlines is shown in figure S7. It can be seen that the streamlines in the bottom of the microfluidic channel follow along the surface groove.

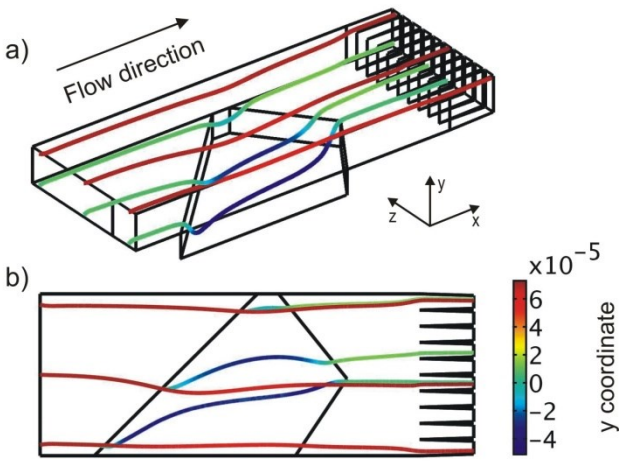

Fig. S7 Schematic of the grooved gradient generator showing the streamlines from 6 starting positions. The colour of the streamlines indicates the y coordinate, i.e. red is close to the channel ceiling while blue is close to the channel floor.

The agent molecules are transported along the streamlines across the width of the microfluidic channel and thus a concentration gradient is generated.

Sensitivity analysis

Figure S8 shows the concentration profiles for the groove geometries which produce the smallest and largest error from the sensitivity analysis in section 3.3 in the main text. The simulated concentration profiles for Graetz numbers between 5 and 150 are shown in figure S9. It can be seen that the concentration profile is almost constant for Gz between 25 and 100.

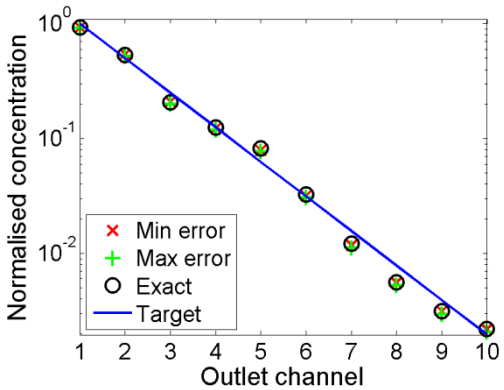

Fig. S8 Concentration profile for varied groove geometries: the concentration profiles for the groove geometries which produce the smallest and largest deviation from the optimal groove configuration are shown. Parameters: Gz=50, ω=2

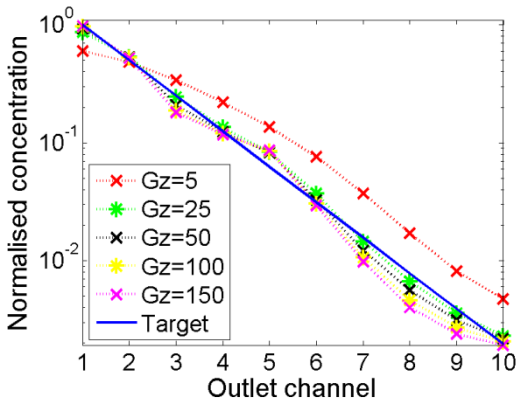

Fig. S9 Simulated concentration profiles for different values of the Graetz number. Parameter: ω=2

Influence of aspect ratio of the channel

Simulations with microfluidic channels with different aspect ratios were investigated. Figure S10 shows the resulting concentration gradient for an aspect ratio of W/H=6 (compared to W/H=4, in the main text) where the same behaviour as the channel studied in the main paper was observed.

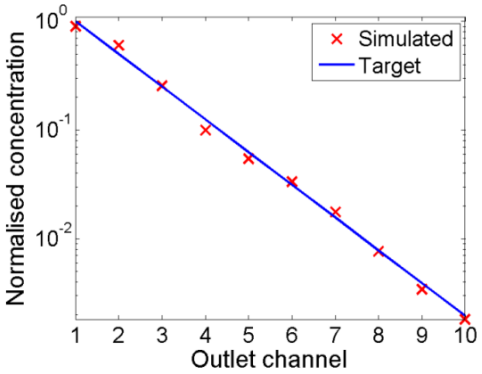

Fig. S10 Simulation results for the exponential concentration gradient in a microfluidic channel with aspect ratio 6. Parameters: Gz=50, ω=2

Influence of groove geometry on the concentration gradient

Several simulations were performed to show the effect of the groove parameters on the concentration gradient. Starting from the groove geometry given by Lynn and Dandy (see reference one parameter at a time is changed to approach the optimal groove found in this contributation. Here only the linear concentration gradient is considered and the inlet width is fixed at 150µm.

For the simple groove geometry the parameters are given in table T2 and the concentration profiles are shown in figure S11. For the complex groove geometry the parameters are given in table T3 and the concentration profiles are shown in figure S12.

Table T2 Groove parameters for concentration profiles shown in figure S11.

	Lynn&Dandy	H_g	L_f	L_n	L_a
H_g	90	71.6	71.6	71.6	71.6
L_f	150	150	217.7	217.7	217.7
L_n	150	150	150	394.5	394.5
L_a	300	300	300	300	360.4

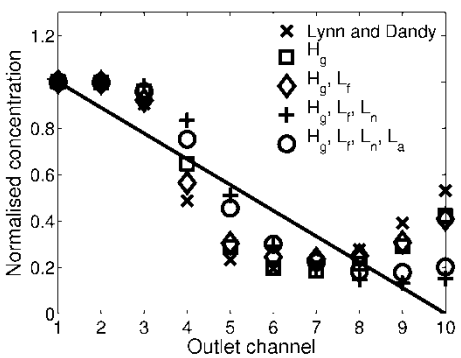

Fig. S11 Simulation showing the approach from the design by Lynn and Dandy to the optimised linear concentration gradient in the simple device.

The results in figure S12 show that the position of the top of the pentagon has a large effect on the concentration profile exiting the channel. Thus the effect of the position of the top of the pentagon is further investigated. Simulations are performed in which the parameters W_m and L_m are increased or decreased by 50µm from the optimal value. See figure S13 for the naming convention and figure S14 and S15 for the results.

Table T3 Groove parameters for concentration profiles shown in figure S12.

	Lynn&Dandy	H_g	L_f	L_n	L_a	W_m	L_m
H_g	90	98.5	98.5	98.5	98.5	98.5	98.5
L_f	150	150	195.0	195.0	195.0	195.0	195.0
L_n	150	150	150	149.5	149.5	149.5	149.5
L_a	300	300	300	300	249.8	249.8	249.8
W_m	150	150	150	150	150	141.2	141.2
L_m	150	150	172.5	172.25	172.25	172.25	377.8

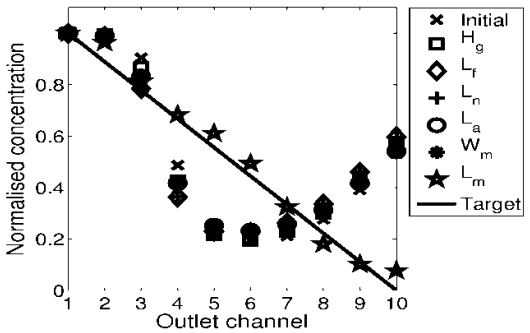

Fig. S12 Simulation showing the approach from the design by Lynn and Dandy to the optimised linear concentration gradient in the complex geometry.

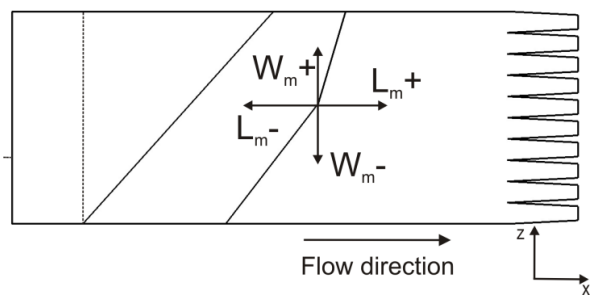

Fig. S13 Schematic of the complex groove design showing the naming convention for the modified pentagon shapes simulated for figures S14 and S15.

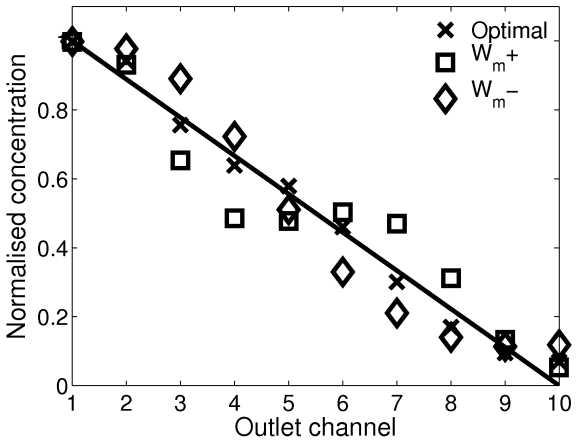

Fig. S14 Simulation showing the resulting linear concentration gradient for the optimal complex design and for two complex grooves with modified lateral positions of the top of the pentagon.

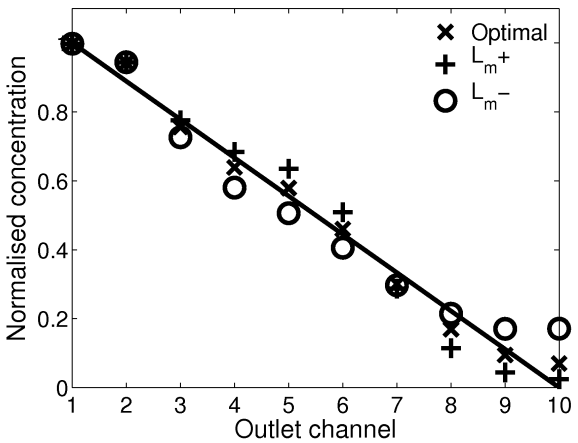

Fig. S15 Simulation showing the resulting linear concentration gradient for the optimal complex design and for two complex grooves with modified axial positions of the top of the pentagon.